

## Article

# A 10.5 ppm/°C Modified Sub-1 V Bandgap in 28 nm CMOS Technology with Only Two Operating Points

Rajasekhar Nagulapalli, Nabil Yassine <sup>\*</sup>, Amr A. Tammam, Steve Barker and Khaled Hayatleh

Faculty of Technology, Design and Environment, School of Engineering, Computing and Mathematics (ECM), Wheatley Campus, Oxford Brookes University, Wheatley OX33 1HX, UK

\* Correspondence: nyassine@brookes.ac.uk

**Abstract:** Reference voltage/current generation is essential to the Analog circuit design. There have been several ways to generate quality reference voltage using bandgap reference (BGR) and there are mainly two types: current mode and voltage mode. The current-mode bandgap reference (CBGR) is widely accepted in industry due to having an output voltage which is below 1 V. However, its drawbacks include a lack of proportional to absolute temperature (PTAT) current availability, a large silicon area, multiple operating points, and a large temperature coefficient (TC). In this paper, various operating points are explained in detail with diagrams. Similar to the conventional voltage mode bandgap reference (VBGR) circuits, modifications of the existing circuits with only two operating points have also been proposed. Moreover, the proposed BGR occupies a much smaller area due to eliminating the complementary to absolute temperature (CTAT) current-generating resistor. A new self-biased opamp was introduced to operate from a 1.05 V supply, reducing systematic offset and TC of the BGR. The proposed solution has been implemented in 28 nm CMOS TSMC technology, and extraction simulations were performed to prove the robustness of the proposed circuit. The targeted mean BGR output is 500 mV, and across the industrial temperature range (−40 to 125 °C), the simulated TC is approximately 10.5 ppm/°C. The integrated output noise within the observable frequency band is 19.6 μV (rms). A 200-point Monte Carlo simulation displays a histogram with a 2.6 mV accuracy of 1.2% (±3-sigma). The proposed BGR circuit consumes 32.8 μW of power from a 1.05 V supply in a fast process and hot (125 °C) corner. It occupies a silicon area of 81 × 42 μm (including capacitors). This design can aim for use in biomedical and sensor applications.



**Citation:** Nagulapalli, R.; Yassine, N.; Tammam, A.A.; Barker, S.; Hayatleh, K. A 10.5 ppm/°C Modified Sub-1 V Bandgap in 28 nm CMOS Technology with Only Two Operating Points.

*Electronics* **2024**, *13*, 1011. <https://doi.org/10.3390/electronics13061011>

Academic Editor: Yahya M. Meziani

Received: 1 January 2024

Revised: 23 February 2024

Accepted: 1 March 2024

Published: 7 March 2024



**Copyright:** © 2024 by the authors. Licensee MDPI, Basel, Switzerland. This article is an open access article distributed under the terms and conditions of the Creative Commons Attribution (CC BY) license (<https://creativecommons.org/licenses/by/4.0/>).

**Keywords:** bandgap reference; noise; operating points; self-bias; offset phase margin

## 1. Introduction

The global semiconductor market, such as IoT and mobile devices, is experiencing tremendous growth in sensors and measuring devices. Every system requires some analogue and mixed-signal blocks to interface the digital and real world [1]. For example, a touch sensor electronics system requires a transducer to convert the finger touch pressure into capacitance. An analogue-to-digital converter (ADC) converts capacitance modulation into digital bits [1,2]. A digital signal processor processes the digital signal (filtering and error correction) and stores it in memory (DRAM/ROM). A digital analogue converter (DAC) can retrieve these stored signals from the real world. Also, audio/video systems require ADC to convert audio signals into digital, and they will playback the voice whenever the user needs a high-quality, low-speed DAC. Sensors often require high dynamic ranges and slow ADCs, whose performance is highly dependent on the quality of the comparator voltage [1–3]. Often, comparators have unacceptable offset and noise, so they need to be trimmed or calibrated efficiently to meet the requirement of signal–noise ratio [3]. In 1 V supply CMOS technology, to design a 10-bit ADC (irrespective of the type of architecture), the least significant bit (LSB) of 1 mV (1/210) should be implemented [1,2]. The errors created in the entire ADC have to be less than half of LSB, so all the errors related to the

noise, mismatch and temperature drift should be less than 0.5 mV. Generally, BGR error contribution is budgeted to 0.25 mV. This will demand high-quality BGR, whose output will be less than 20–25 ppm/°C ppm. Also, the noise of the bandgap reference must be very low, and the frequency band is limited to the sampling rate of the ADC (ranging from 10 Ms/s to 24 Gs/s) [1,2]. Low dropout regulators (LDO) are required to power all the highly sensitive analogue circuits; they need a high-quality, low-noise reference voltage, which the BGR will supply. Usually, the BGR current will be routed to the input of the LDO, where it will be converted into the voltage using a potential divider followed by a low-cutoff-frequency RC filter to improve the thermal-noise performance. Such high-quality reference voltages are generated by the bandgap reference circuit (BGR) [1]. Brokaw [4] first proposed the VBGR principle in BJT technology. It is essentially a scaled sum of a proportional to absolute temperature (PTAT) voltage and a complementary to absolute temperature (CTAT) voltage. The BJT's base-emitter voltage ( $V_{BE}$ ) has a negative temperature gradient of 2 mV/°C, which can be used as the CTAT voltage. Though VBE has nonlinear curvature in its equation, it is commonly approximated with a linear term for the first-order temperature sensitivity [5,6]. The actual slope is a strong function of diode doping and what kind of current has been used to bias the device [4]. The VBE difference between two BJTs with different current densities has a positive slope and can be used as a PTAT. For a current density ratio of eight, the PTAT voltage slope is around 100  $\mu$ V/°C. One should equalise the PTAT and CTAT temperature sensitivities for low-temperature sensitivity [1]. Hence, the PTAT voltage must be amplified by 20 and added to the CTAT voltage. Brokaw's design [4] uses BJT technology and creates the voltage at the collector of the BJT; unfortunately, this proposal is very sensitive to the BJT's base current despite the BJT's large current gain. Later, a CMOS technology-based BGR was created using vertical parasitic PNP devices (poor current gain). The BJT-based VBGR works well but requires a power supply above 1.8 V, and its output voltage should not operate below 1.23 V [1].

In 1975, the semiconductor-integrated chip revolution started, and Intel accelerated chip development in terms of the product's features and the number of transistors [4]. Robert More noticed that the number of transistors in a chip is almost doubled in either a 12-month or 18-month time frame. This observation has been termed "Moore's Law", which has dictated semiconductor manufacturing technology. Every fab, for example, Intel or Taiwan Semiconductor Manufacturing Corporation (TSMC), used the rule to improve technology. Since the target is to increase the transistor number by 2-fold in the same area, each transistor area must decrease by 0.5-fold [7]. Generally, each transistor is similar to a square shape (almost every transistor, but there are few exceptions). Hence, transistor width and length should go decrease by approximately 0.707-fold.

Decreasing the length of the transistor is referred to as scaling [4]. With scaling, several challenges appeared, and device engineers solved those problems by changing the transistor doping and different materials for constructing the transistor (device engineering). After 45 nm technology CMOS, the technology name no longer defined the transistor dimension. Instead, it was the smallest pitch of the dynamic random-access memory (DRAM) fabricated in the technology or the minimum spacing between the side-by-side of the lowest possible metal layer (typically  $M_1$ ). Also, with the scaling of the transistor size, the metal thickness has decreased to cope with the transistor scaling pace [4]. Unfortunately, passive devices like resistors, capacitors (metal oxide metal type), and inductors cannot be scaled, as they are a physical property of the material. That is why there has been a trend to construct the analogue circuit with a minimum number of passive components and sometimes emulate the passive properties with transistor biasing [7]. For example, a resistor can be replaced with an NMOS transistor, biased in the triode region, with very little draining to the source voltage. An inductor can be synthesised using a transistor with some resistance in series with the gate, such that its impedance will increase with its frequency [7].

In today's industry, downscaling the dimensions of CMOS transistors has accelerated, aiming to improve the microprocessor's digital processing capacity [4]. This is achieved by decreasing the capacitance and improving the operating frequency of transistors. There

has been constant voltage and electric field scaling, with most manufacturing organisations preferring a constant electric field to maintain chip reliability [4]. Unfortunately, to keep the electric field inside the device, there needs to be a decrease in the power supply voltage, which is continuously reduced to keep the electric field between the drain and the source of the transistor constant. Also, scaling leads to a substantial increase in the leakage of the off-state transistor because gate oxide becomes thinner and is susceptible to tunnel phenomena [4]. So, device engineers increased the transistor's threshold voltage ( $V_{TH}$ ) to counteract this leakage issue. A lower supply voltage and higher  $V_{th}$  can lead to many challenges in analogue design. The common-mode voltage requirement of the opamp or any analogue circuit will be very high due to the high  $V_{th}$  and the low supply. Hence, it is not easy to reach a decent amount of gain [7]. Also, due to the decrease in the device size, the mismatch among the devices is a severe threat to the analogue design regarding the accuracy of the current mirror gain and offset of the differential pairs. Dynamic offset cancellation techniques like chopping or dynamic element matching (DEM) will often be exploited to improve the offset of the circuits [7]. Chopping is swapping the bias currents of the differential pair from one side to another over time so that the offset of devices will be converted as high-frequency systematic noise, which the notch filter can filter. However, chopping introduces several non-ideal characteristics, such as the input current of the opamp and high-frequency noise in the output of the circuit. Therefore, there is a great deal of interest in finding ways to lower the BGR output voltage without using dynamic circuit techniques [8]. The proposed current-mode bandgap reference (CBGR) by P. Brokaw [4] has the advantage of operating at zero TC current by summing the CTAT and PTAT currents, providing an output voltage of less than 1 V and requiring less supplied voltage [9,10]. Unfortunately, CBGR has drawbacks, such as occupying a large silicon area and having an offset gain. H. Banba et al. [7] proposed modification of the current-mode BGR to eliminate the undesirable operating point by creating a resistor mismatch. However, it will produce a larger TC because of the current deviation in both BJTs of the BGR. The mixed-mode BGR circuit proposed by Yu and L. Siek [11] to improve TC requires a slightly higher supply voltage and exhibits a poor TC. Also, a few applications, such as VCO and amplifiers, require a PTAT current to eliminate the temperature degradation of the circuit parameters. There have been several improvements made by providing additional PTAT current. All the presented literature lacks separate PTAT current sources while providing the sub-1 V output. A. J. Annema et al. [12] proposed a mixed-mode BGR, which mixes the PTAT current and CTAT voltage. Yat-Hei Lam et al. [13] and A. J. Annema [12] proposed work that has some modifications of the existing ones, either by adding current summation or implementing curvature compensation [14,15]. In Yat-Hei Lam et al.'s [13] proposed research, the PTAT current and CTAT voltage were added using a resistor and BJT. Still, they did not improve TC much, especially since the systematic offset of BGR was not addressed. A. J. Annema et al. [12] proposed a bandgap with a resistive divider at the input of the opamp so that the opamp experiences a very low common mode at a high temperature to improve performance [16]. Unfortunately, this technique increases the mismatch due to additional potential division. In addition, the input offset of the opamp will be amplified by the attenuation of the divider.

The research presented in this paper proposes a novel BGR with a very small silicon area compared to the prior design and a high-gain self-biased opamp to address the systematic offset-induced TC.

The paper is divided into six sections. Section 2 (following the introduction in Section 1) describes the working principle CBGR and a graphical explanation of the existing multiple-operating-point problem. Section 3 compares the proposed BGR circuit and previous conventional circuits and their derivatives. Section 4 describes the BGR design. Section 5 summarises the post-layout simulation results compared with the existing state-of-the-art simulation. Finally, Section 6 includes the conclusions drawn from the research presented here.

### 2. Conventional Current-Mode BGR

Figure 1 shows a conventional current-mode BGR. Q1, Q2, and R1 form the BGR core cell, and the area of Q2 is *n* times that of Q1 [17]. The operational amplifier (op1) modulates the current through the BJT so that the potentials at nodes X and Y are equal, and the current density difference in Q1 and Q2 causes the voltage across R1 to have PTAT behaviour. The current through R1, R2 can be expressed as

$$I_{R1} = \frac{V_T \ln n}{R_1}, \tag{1}$$

$$I_{R2} = \frac{V_{BE1}}{R_2}, \tag{2}$$

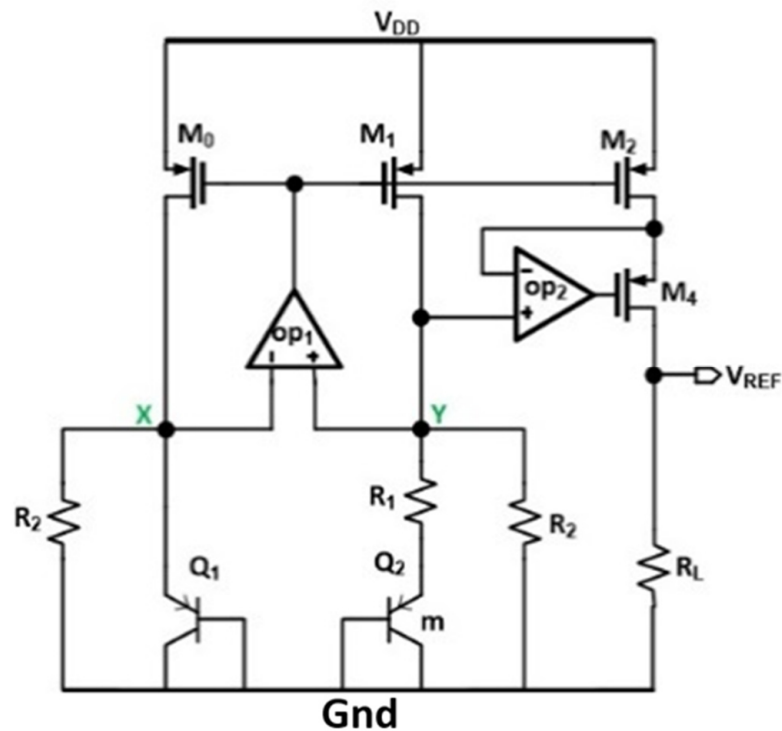


Figure 1. A conventional current-mode bandgap schematic [17].

The output current through M2 is the sum of  $I_{R1}$  and  $I_{R2}$ . The CTAT current has a TC of  $-2 \text{ mV}/^\circ\text{C}$  and a PTAT of  $25 \text{ } \mu\text{V}$  (for  $n = 24$ ). Therefore, we need to amplify the PTAT currents so that TC is zero after summing. The output voltage can be expressed as shown in (3) [17].

$$V_{Ref} = \frac{R_L}{R_2} \left[ \frac{R_2}{R_1} V_T \ln n + V_{BE1} \right] \tag{3}$$

By adjusting the ratio of  $R_2$  and  $R_1$  to minimise TC and adjusting  $R_L$  to generate the desired output voltage. This CBGR is simple and provides an output voltage of less than 1 V, but it has some problems. The  $R_2$  required for zero TC is very large. For example, to bias the BG core to  $3 \text{ } \mu\text{A}$ , the values of  $R_1$  and  $R_2$  should be  $17 \text{ k}\Omega$  and  $198 \text{ k}\Omega$ , respectively. Such a large value of  $R_2$  occupies a lot of active space, and there are also two instances of  $R_2$ , and hence, this is an area-in-efficient [4,17]. Conventionally, the VBGR has two operating points, a desired and an undesired operating point (zero current). Therefore, a start-up circuit prevents the circuit from getting stuck at zero current. In contrast, CBGR has multiple operating points. This is because when the bandgap core carries little current, Q1 Q2 will not turn on, and most of the current will flow through  $R_2$  (Figure 1). Therefore, op1 opamp will sense zero differential voltage until the current is large enough to turn on the BJT. To

quantify the operating point, replace  $M_0$  and  $M_1$  with ideal current sources, you must sweep their values from 0 to 10  $\mu\text{A}$ , and plot the differential input voltage of the opamp as in Figure 2. At a maximum bias current of 1.4  $\mu\text{A}$ , the opamp input terminals will see the same voltage (meaning the BJT is not turned on), indicating that the BGR can operate at any current within 1.4  $\mu\text{A}$  (some undesirable points). When the current exceeds 1.4  $\mu\text{A}$ , the Q1–2 device turns on, and the voltages of nodes X, Y are different for the same current. As soon as the current approaches 8  $\mu\text{A}$ , the opamp  $op_1$  input becomes 0 V again, so this is also the operating point (preferred). To avoid these problems, a starter circuit is necessary, and designing the starter circuit is difficult due to the above-mentioned points. It uses a POR circuit to avoid the failure of this circuit [18]. A small asymmetry in the opamp is used, as shown in Equation (3) (intentionally adding a mismatch to  $R_2$ ) [11]. This circuit does not have access to the PTAT current like the VBGR circuit, so if PTAT is required, it must be generated by additional circuitry at the cost of more current and mismatch, as given in Equation (4). This architecture also amplifies that there is opamp offset with a large gain compared to the traditional BGR due to the resistor loaded on the input terminal of the opamp. Therefore, a larger gain will amplify any residual input-related offset and affect the output TC. Equations (4) and (5) show the output voltage due to only the opamp offset in VBGR and current-mode BGR, respectively [17].

$$V_{out} = V_{os} \left( 1 + \frac{R_2}{R_1} \right), \quad (4)$$

$$V_{out} = V_{os} \left( 1 + \frac{R_2}{R_1} + \frac{R_L(R_1 + R_2)}{R_1 R_2} \right), \quad (5)$$

According to the authors, the bandgap core is of a low current and symmetrical, which causes the circuit to stall at some operating point. Therefore, removing  $R_2$  makes the circuit asymmetrical at all currents and reduces the loading of  $R_2$  on the opamp input. Therefore, removing  $R_2$  minimises the number of operating points. The main purpose of  $R_2$  is to eliminate multi-operating points and ensure only two operating points [17].

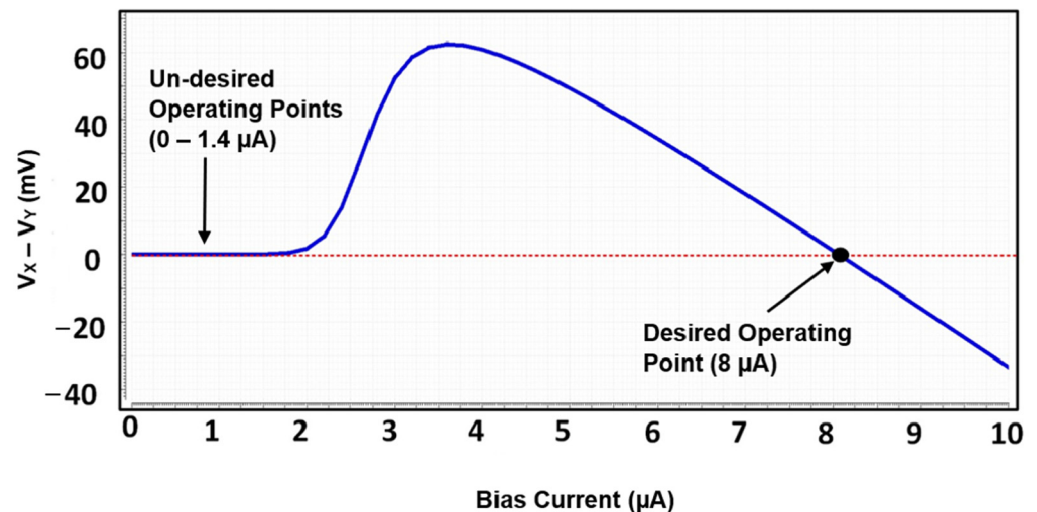


Figure 2. Simulation results for the opamp's  $op_1$  differential input voltage versus BGR core bias current [17].

### 3. Proposed Technique

Figure 3 shows the proposed architecture circuit, which consists of two sections. One is a BGR core that generates a PTAT stream consisting of  $Q_1$ ,  $Q_2$ ,  $OP_1$ ,  $M_0$ ,  $M_1$ ,  $R_p$ , and the other is a stream adder consisting of  $OP_2$ ,  $M_4$ , and  $R_2$ . Note that the start circuit is not shown here for simplicity. Compared to the conventional VBGR, this proposal uses the base connection to generate the PTAT current, thus achieving a kind of curvature

compensation [11]. Since the voltage across  $R_p$  is  $V_{BE2}-V_{BE1}$ , it has a PTAT characteristic. The operational amplifier ( $OP_2$ ) sets the gate voltage of  $M_4$  such that  $V_X = V_Y$ . Therefore, the voltage across  $R_2$  will be  $V_{BE2}$ , and the current through  $R_2$  will have the properties of CTAT.  $M_2$  carries a sum of PTAT and CTAT currents that allows the TC to be set to zero by adjusting the ratio of  $R_2$  and  $R_p$ . The output voltage is given using Equation (6).

$$V_{BG} = \frac{R_3}{R_2} \left[ V_{BE2} + \frac{R_2}{R_p} V_T \ln n + V_{os} \left( 1 + \frac{R_2}{R_p} \right) \right] \tag{6}$$

where  $V_{os}$  is the  $OP_1$  offset.

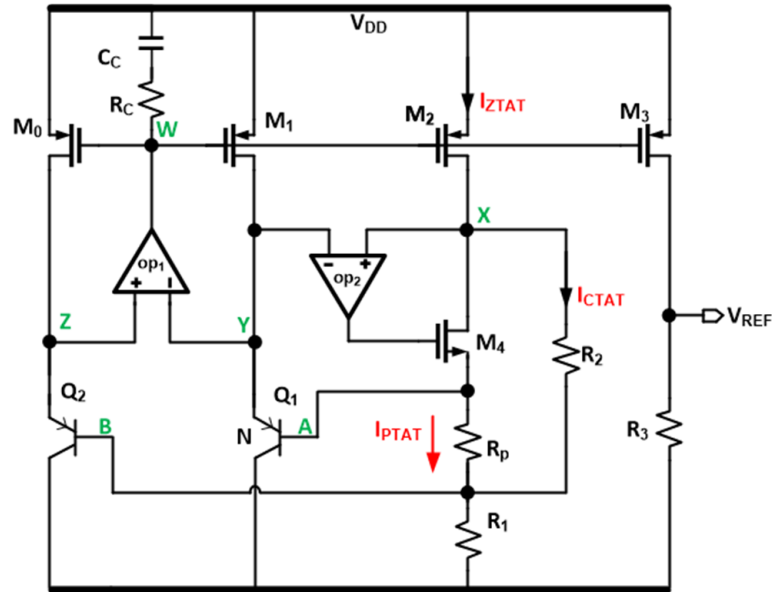


Figure 3. Schematic of the proposed mixed-mode BGR circuit. The green letters are arbitrary nodes, while the red arrows indicate the respective direction of the current.

Resistor  $R_1$  is not required in this circuit, but its voltage has a non-linear temperature dependence due to the base current, which improves TC. However,  $R_1$  increases the minimum power supply required by the circuit, so  $V_{R1} < 30$  mV for this current research. Even at very low bias currents, the opamp input nodes experience different impedances, so there is no unwanted operating point other than zero current. This is a major advantage of the proposed BGR compared to CBGR. The new proposed circuit has a smaller silicon area than the CBGR (up to 29% savings in silicon area), as only one CTAT register is used. Since  $R_2$  does not load the  $OP_1$  input, the opamp offset voltage is amplified by the gain, given in Equation (4), which is less than the current-mode BGR. A voltage source was connected to the opamp output (node w), shifted its value from 0 to  $V_{DD}$ , and plotted the current through the voltage source to show the number of operating points. The number of current zero crossing points indicates the number of operating points. Figure 4 shows the current through the voltage source added in the testbench. Since there is only one crossing point in 200 Monte Carlo simulations, this new proposal circuit successfully eliminates all unnecessary operating points (because of the start-up circuit; thus, there is no zero current point).

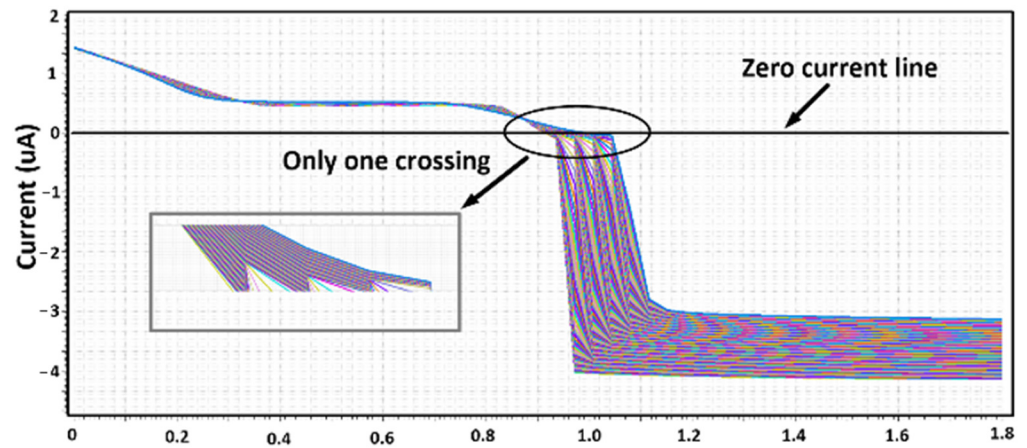


Figure 4. Voltage source current versus voltage of different Monte Carlo simulation runs.

#### 4. Self-Bias Opamp and Design Techniques

The systematic offset of OP1 plays a significant role in BGR performance with respect to temperature [19,20]. Equation (6) shows that VOS is amplified using a ratio of  $\frac{R_2}{R_p}$  due to the closed-loop nature of the BGR, and this amplification factor is so large that it might impact the TC of the output voltage. Unfortunately, the opamp offset temperature sensitivity is unknown; otherwise, it could be corrected similarly to the output voltage. If the opamp tail current was biased with the constant current, then the opamp output common-mode voltage will have a different nature than the bandgap PMOS current sources. One way to reduce/solve this problem is to bias the opamp with the BGR core current [21,22]. This gives the current mirror gain because the opamp output matches the desired output voltage (vdd-vsg, p). The ratio will be close to one. Figure 5a shows the conventional self-bias scheme, which works as follows.  $M_0, M_1, M_7, M_9, M_{10}$  form the current source load opamp. The node Y voltage has been sensed with  $M_2$  and  $M_5$  and drives the opamp tail current source gate with a low pass filter. The low pass filter is an essential part of the self-bias as it will slow down the self-bias loop such that for the main BGR loop, the opamp current is a static parameter. The loop gain of the self-bias depends on the ratio of  $g_{m2}$  and  $m_5$ . The main purpose of the self-bias loop is to make the x,y node potential as close as possible. Unfortunately, due to the limited gain in the self-bias loop, they will be better than the fixed bias opamp, but still, there is room for improvement. Figure 5b depicts the proposed opamp bias structure, where the gain from node x,y to node z has been increased significantly. An opamp has been deployed from nodes x,y to node z to considerably enhance loop gain, reducing the steady state error between the node x,y potentials. The loop gain can be expressed as follows (7). The loop gain has dominated the pole associated with the low pass RC filter, which keeps the other opamp poles far away, such that the phase margin is close to  $90^\circ$  (this phase margin differs from the main loop). Compared to Figure 5a, this circuit loop gain is almost 30 dB higher (higher than  $(\frac{g_{m2}}{g_{ds5} + g_{ds2}})$ ).

$$lg = \frac{g_{m2}}{g_{ds5} + g_{ds2}} \frac{g_{m7}}{g_{m1}} \quad (7)$$

The often  $V_{DS}$  mismatch of the self-bias will have minor errors in the final settling. Hence, the M4 device has been introduced to match the bias network  $V_{DS}$  to the main opamp.

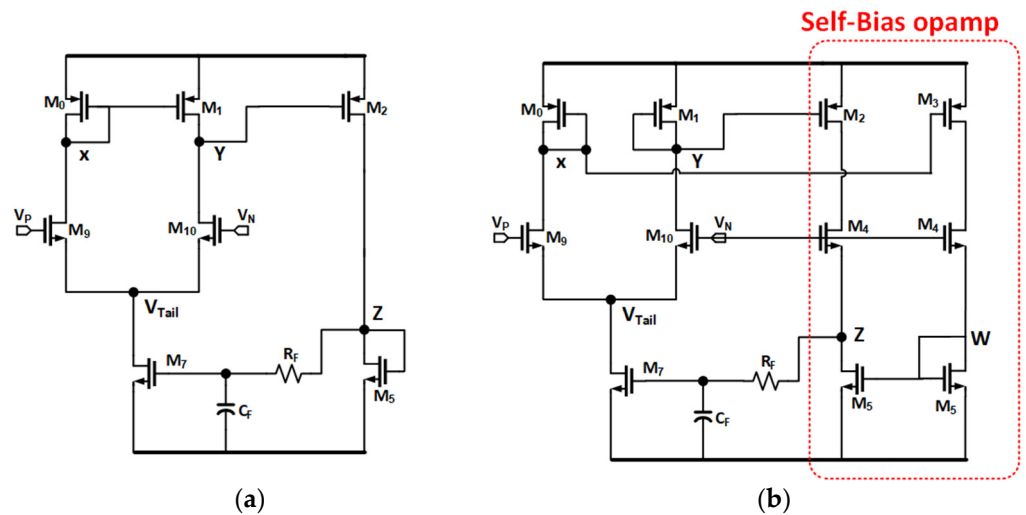


Figure 5. Self-bias opamp schematic for (a) a conventional circuit and (b) the proposed circuit.

### 5. Simulation Results

The proposed BGR was implemented in TSMC 28 nm low-power (LP) CMOS technology, which has 10 metals and one poly layer. A low-power process means there is very little leakage current in the off state of the transistor; hence, the threshold voltage of the transistor would be a little higher [23]. This process contains core and IO transistors to support low- and high-voltage supply. Post-layout simulations based on a resistor coupling capacitor-extracted netlist were performed across NMOS and PMOS typical, NMOS and PMOS fast, NMOS and PMOS slow, fast NMOS and slow PMOS, and slow NMOS and fast PMOS corners. Also, the simulations assumed the PAD capacitance and parasitic interface while connected to the PCB. BGR draws 31.23  $\mu\text{A}$  from the 1.05 V supply. Figure 6 shows the output voltage versus temperature for process corners (TT, FF, SS) and resistance corners (high and low). The output voltage varies from 496.8 to 503 mV over the industrial temperature range ( $-40\text{ }^\circ\text{C}$  to  $125\text{ }^\circ\text{C}$ ) with a TC of 10.5 ppm/ $^\circ\text{C}$  at the FF corner. An interesting observation is that the output voltage is more sensitive to the resistance corner than the MOS corner at a given temperature because the bias current in the BGR core is proportional to  $R_P$ , which will be changed [23]. Therefore, two sets of output plots in Figure 6 correspond to the resistance corners.

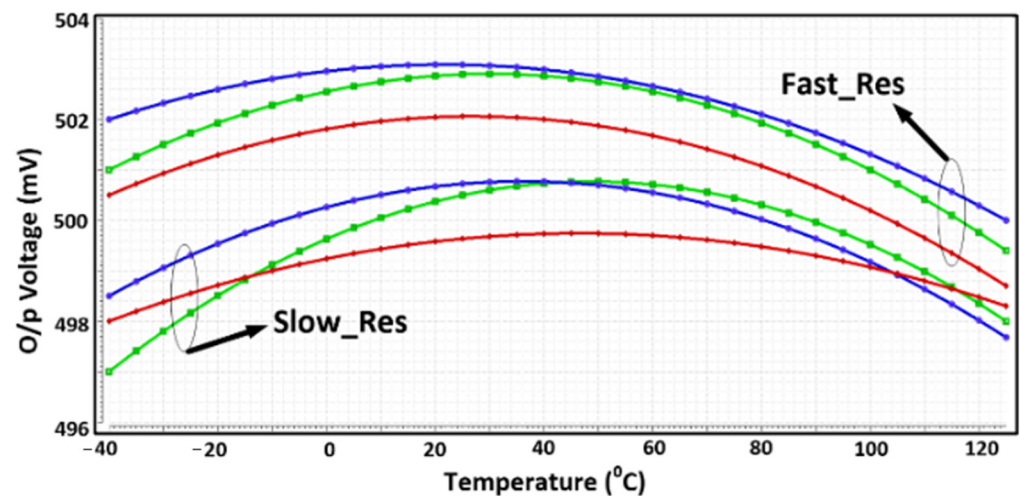


Figure 6. Two sets of Output plots showing voltage vs. temperature across PVT of the resistance corners.

Figure 7 shows the output's simulated noise power spectral density and the integrated RMS noise of  $\sim 19.4 \mu\text{V}$ . Most of the noise is contributed by OP1, Rp, and M0. More importantly, the noise in OP1 is multiplied with  $R1/Rp$ . This was reduced by choosing a higher  $n$  so that there is less of the multiplication factor, but the trade-off with a very high  $n$  increases the risk of the reverse saturation current. Figure 8 shows a simulated histogram of the output voltages corresponding to 6-Sigma 200 Monte Carlo simulations [24], indicating a standard deviation of  $1.98 \text{ mV}$  and an accuracy of  $1.21\%$ . Note each point in the histogram is a single Monte Carlo simulation. Figure 9 shows the simulated gain and phase of the proposed self-bias opamp [25].

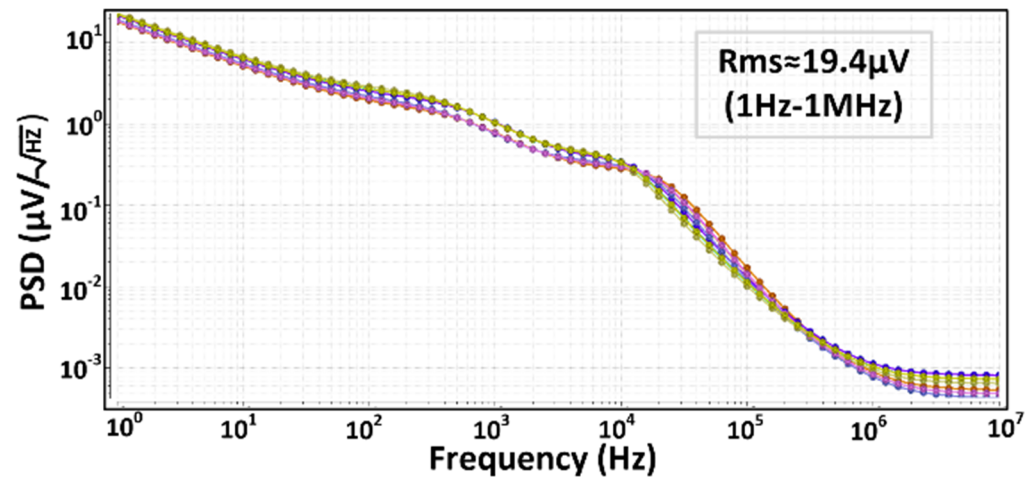


Figure 7. Simulated power spectral density of the BGR PVT Corners.

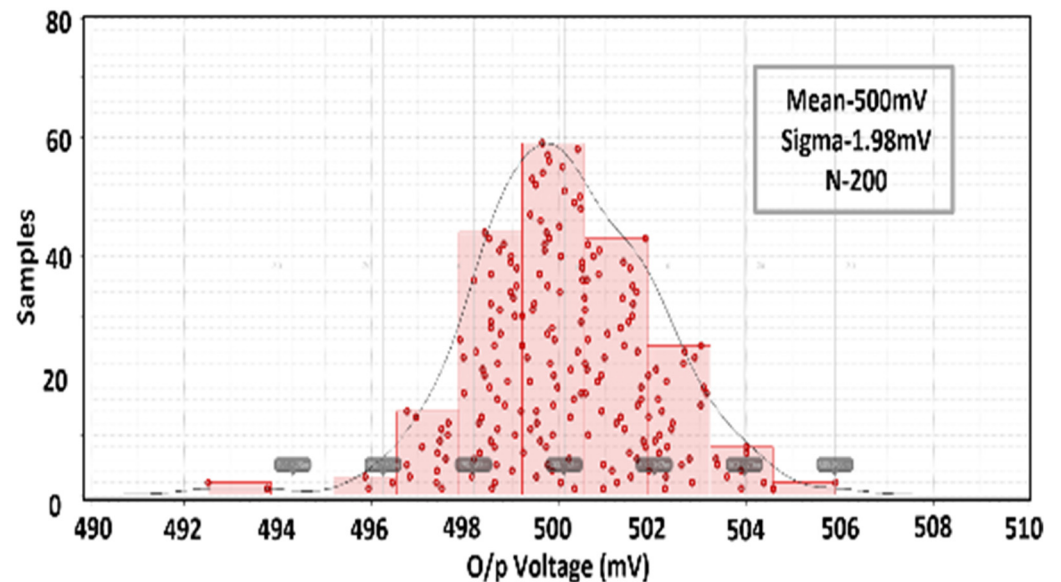
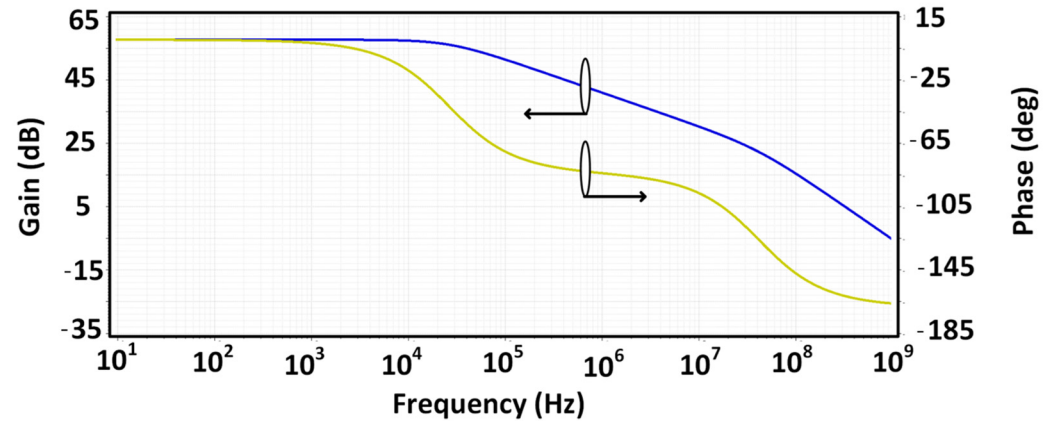


Figure 8. 6-Sigma 200 Monte Carlo simulations Histogram of the Output voltage vs. temperature across PVT.

Figure 10 shows the layout of the proposed circuit. It has a surface area of  $81 \times 42 \mu\text{m}^2$ , including decoupling capacitors and dummy devices, most of which are dominated by the current source OPAMP (OP1) and PMOS [26–28]. The proposed design has a lower temperature coefficient compared to the designs by Yu and L. Siek [7], A. J. Annema [12], and Yu and J. Lee [29], as shown in Table 1.

A. J. Annema [12] reached a lower supply voltage ( $0.15 \text{ V}$  less) and power consumption ( $38.4\%$  less) compared to the proposed work. However, this came at a much higher

temperature coefficient (95.2 times more) and generated 3.04 times more noise. The design by Yu and L. Siek [7] generated less noise compared to the proposed design but came at the cost of a higher supply voltage (0.75 V), higher temperature coefficient (2.5 ppm/°C), and consumed 3.01 times more power.



**Figure 9.** Gain and phase of the self-bias loop opamp. The yellow graph shows the phase response. The blue graph shows the magnitude frequency.

Lastly, the design by J. Lee [29,30] underperformed compared to the proposed design in terms of the supply voltage (0.375 V more needed), temperature coefficient (3.9 times more), and power (1.7 times more), as shown in Table 1. This layout was designed for the sake of extracted simulations, not for manufacturing. Hence, we did not include pads/bumps or package-related parasitic elements [31–34].

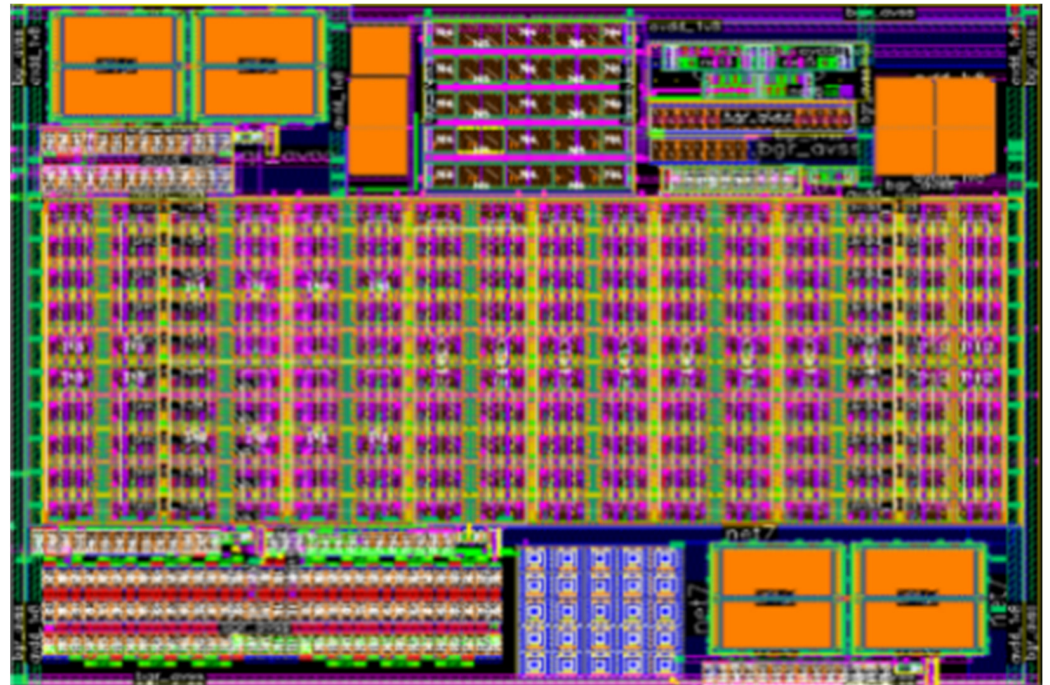


**Figure 10.** Layout of the proposed circuit.

**Table 1.** Comparison with the existing state-of-the-art circuits.

Parameter	Unit	[12]	[7]	[29]	Proposed Work
Technology	nm	32	160	45	28
Supply Voltage	V	0.9	1.8	1.425	1.05
Temperature Coefficient (TC)	ppm/°C	1000	12	41	10.5
Noise	μV	59	6.1	--	19.4
Circuit Power consumption	μW	12.6	99	57	32.8

## 6. Conclusions

High accuracy and low TC bandgaps are very important in sensor/measurement applications. This paper analyses the current-mode bandgap reference circuit graphically and explains the existing problems qualitatively. A new style of bandgap, which is very compact and produces sub-1 V output voltage, has been proposed. Fabrication of the proposed circuit is currently not planned until more research is carried out and funding is obtained.

The proposed circuit has a TC of 10.5 ppm/°C, eliminated multiple operating points, and decreased the silicon area by reducing the number of resistors. The proposed work outperforms the state-of-the-art technologies proposed by Yu and L. Siek [7], A. J. Anema [12], and Yu and J. Lee [29] (Table 1) by having a lower temperature coefficient. The proposed work is also competitive regarding the supply voltage, the power requirements, and the noise generated. The proposed design was developed using 28 nm CMOS technology. According to the authors, this performance is suitable for audio/biomedical sensing applications requiring 20-bit digital performance.

**Author Contributions:** Writing—original draft preparation, R.N.; Writing—review and editing, N.Y., A.A.T., S.B. and K.H. All authors have read and agreed to the published version of the manuscript.

**Funding:** This research received no external funding.

**Data Availability Statement:** Data is contained within the article.

**Conflicts of Interest:** The authors declare no conflict of interest.

## References

- Nagulapalli, R.; Palani, R.K.; Bhagavatula, S. A 24.4 ppm/°C Voltage Mode Bandgap Reference with a 1.05V Supply. *IEEE Trans. Circuits Syst. II Express Briefs* **2021**, *68*, 1088–1092. [\[CrossRef\]](#)
- Tian, H.; Yi, T. High Precision Voltage Reference for ADC: Review and Design Methodology. In Proceedings of the 2022 7th International Conference on Integrated Circuits and Microsystems (ICICM), Xi'an, China, 28–31 October 2022; pp. 225–229.
- Hosny, A.; Farag, F.A.; Wahba, A.; Mohamed, A.R. A power-efficient dynamic-time current mode comparator. *AEU Int. J. Electron. Commun.* **2023**, *171*, 154934. [\[CrossRef\]](#)
- Brokaw, P. A simple three-terminal IC bandgap reference. *IEEE J. Solid-State Circuits* **1974**, *9*, 388–393. [\[CrossRef\]](#)
- Boni, A. Opamps and startup circuits for CMOS bandgap references with near 1-V supply. *IEEE J. Solid-State Circuits* **2002**, *37*, 1339–1343. [\[CrossRef\]](#)
- Fu, X.; Colombo, D.M.; Yin, Y.; El-Sankary, K. Low Noise, High PSRR, High-Order Piecewise Curvature Compensated CMOS Bandgap Reference. *IEEE Access* **2022**, *10*, 110970–110982. [\[CrossRef\]](#)
- Banba, H.; Shiga, H.; Umezawa, A.; Miyaba, T.; Tanzawa, T.; Atsumi, S.; Sakui, K. A CMOS bandgap reference circuit with sub-1-V operation. *IEEE J. Solid-State Circuits* **1999**, *34*, 670–674. [\[CrossRef\]](#)
- Lee, J.; Kim, C.-S.; Choi, J.H.; Kim, K.S.; Koo, B.T. Untrimmed BGR of 1.1% 3σ Based on Dynamic-Biased Op Amp with Reduced Voff. *IEEE Trans. Circuits Syst. II Express Briefs* **2020**, *67*, 1829–1833. [\[CrossRef\]](#)
- Naganadhan, V.; Saikiran, M.; Gshash, M.; Chen, D. Systematic Methodology to Design High Precision Voltage References with Sub-ppm/°C Temperature Coefficient. In Proceedings of the 2023 IEEE East-West Design & Test Symposium (EWDTS), Batumi, Georgia, 22–25 September 2023; pp. 1–11.

10. Wang, X.; Bai, C. Design of a Bandgap Reference Circuit with Ultra-low Temperature Coefficient. In Proceedings of the 2021 IEEE 14th International Conference on ASIC (ASICON), Kunming, China, 26–29 October 2021; pp. 1–4.
11. Yu, C.; Siek, L. An Area-Efficient Current-Mode Bandgap Reference with Intrinsic Robust Start-Up Behavior. *IEEE Trans. Circuits Syst. II Express Briefs* **2015**, *62*, 937–941. [[CrossRef](#)]
12. Annema, A.J.; Veldhorst, P.; Doornbos, G.; Nauta, B. A sub-1 V bandgap voltage reference in 32 nm FinFET technology. In Proceedings of the 2009 IEEE International Solid-State Circuits Conference—Digest of Technical Papers, San Francisco, CA, USA, 8–12 February 2009; pp. 332–333.
13. Lam, Y.-H.; Ki, W.-H. CMOS Bandgap References with Self-Biased Symmetrically Matched Current–Voltage Mirror and Extension of Sub-1-V Design. *IEEE Trans. Very Large Scale Integr. (VLSI) Syst.* **2010**, *18*, 857–865. [[CrossRef](#)]
14. Huang, S.; Li, M.; Li, H.; Yin, P.; Shu, Z.; Bermak, A.; Tang, F. A Sub-1 ppm/°C Bandgap Voltage Reference with High-Order Temperature Compensation in 0.18- $\mu$ m CMOS Process. *IEEE Trans. Circuits Syst. I Regul. Pap.* **2022**, *69*, 1408–1416. [[CrossRef](#)]
15. Ye, J.; Mao, D.; Zheng, W. Design of a Low Temperature Drift High Power Supply Rejection Bandgap Reference Circuit. In Proceedings of the 2023 IEEE 15th International Conference on ASIC (ASICON), Nanjing, China, 24–27 October 2023; pp. 1–4.
16. Hande, V.; Shojaei Baghini, M. Survey of Bandgap and Non-bandgap based Voltage Reference Techniques. *Sci. Iran.* **2016**, *23*, 2845–2861. [[CrossRef](#)]
17. Nagulapalli, R.; Palani, R.K. A 4.5X Noise Improved Split-Resistance Current mode Bandgap with 18.4 ppm/°C in 28 nm CMOS. In Proceedings of the 2023 34th Irish Signals and Systems Conference (ISSC), Dublin, Ireland, 13–14 June 2023; pp. 1–4.
18. Palani, R.K.; Nagulapalli, R.; Bhagavatula, S. Dynamic Averager Based Sub-1V Bandgap Voltage Reference. In Proceedings of the 2023 IEEE 66th International Midwest Symposium on Circuits and Systems (MWSCAS), Tempe, AZ, USA, 6–9 August 2023; pp. 890–894.
19. Haq, S.U.; Abbasian, E.; Sharma, V.K.; Khurshid, T.; Fathi, H. Energy-Efficient High-Speed dynamic logic-based One-Trit multiplier in CNTFET technology. *AEU Int. J. Electron. Commun.* **2024**, *175*, 155088. [[CrossRef](#)]
20. Shen, J.; Diao, S. A Sub-1 ppm/°C TC Bandgap Voltage Reference with High Power Supply Rejection. In Proceedings of the 2022 15th International Congress on Image and Signal Processing, BioMedical Engineering and Informatics (CISP-BMEI), Beijing, China, 5–7 November 2022; pp. 1–4.
21. Nagulapalli, R.; Hayatleh, K.; Barker, S.; Reddy, B.N.K.; Seetharamulu, B. A High Frequency CMRR improvement technique for Differential Amplifiers in 45 nm CMOS. In Proceedings of the 2019 10th International Conference on Computing, Communication and Networking Technologies (ICCCNT), Kanpur, India, 6–8 July 2019; pp. 1–5.
22. Saweth, H.; Sa-Ngiamvibool, W.; Aurasopon, A. Design of bandgap core and startup circuits for all cmos bandgap voltage reference. *Prz. Elektrotechniczny* **2012**, *88*, 277–280.
23. Nagulapalli, R.; Hayatleh, K.; Barker, S.; Zourob, S.; Yassine, N.; Reddy, B.N.K. High Performance Circuit Techniques for Nueral Front-End Design in 65 nm CMOS. In Proceedings of the 2018 9th International Conference on Computing, Communication and Networking Technologies (ICCCNT), Bengaluru, India, 10–12 July 2018; pp. 1–4.
24. Moiselto, E.; Ippolito, C.M.; Bruno, G.; Malcovati, P.; Bonizzoni, E. A MOS-Based Temperature Sensor with Inherent Inaccuracy Reduction Enabled by Time-Domain Operation. *IEEE Trans. Instrum. Meas.* **2023**, *72*, 2004110. [[CrossRef](#)]
25. Ker, M.-D.; Chen, J.-S.; Chu, C.-Y. New curvature-compensation technique for CMOS bandgap reference with sub-1-V operation. In Proceedings of the 2005 IEEE International Symposium on Circuits and Systems (ISCAS), Kobe, Japan, 23–26 May 2005; pp. 3861–3864.
26. Hoang, T.; Quoc, T.N.; Zhang, L.; Duong, T.Q. Novel Methods for Improved Particle Swarm Optimization in Designing the Bandgap Reference Circuit. *IEEE Access* **2023**, *11*, 139964–139978. [[CrossRef](#)]
27. Zhou, Z.; Yu, H.; Shi, Y. A Time-domain Bandgap Reference with Continuous Output Voltage. In Proceedings of the 2018 IEEE Asia Pacific Conference on Circuits and Systems (APCCAS), Chengdu, China, 26–30 October 2018; pp. 476–479.
28. Banerjee, S.; Chatterjee, S.; Mukherjee, K.; Pandit, S. A Temperature Compensated Beta-Multiplier Based Sub-1 V Voltage Reference Circuit for Low-Voltage Applications. In Proceedings of the 2023 IEEE Devices for Integrated Circuit (DevIC), Kalyani, India, 7–8 April 2023; pp. 291–295.
29. Anushree; Kaur, J. Comparative study of Curvature Correction in CMOS Bandgap Reference Circuit. In Proceedings of the 2020 IEEE 17th India Council International Conference (INDICON), New Delhi, India, 10–13 December 2020; pp. 1–4.
30. Huang, Y.; Zhu, L.; Kong, F.; Cheung, C.; Najafzadeh, L. BiCMOS-Based Compensation: Toward Fully Curvature-Corrected Bandgap Reference Circuits. *IEEE Trans. Circuits Syst. I Regul. Pap.* **2018**, *65*, 1210–1223. [[CrossRef](#)]
31. Grasso, A.D.; Pennisi, S.; Venezia, C. 28-nm CMOS Resistor-Less Voltage Reference with Process Corner Compensation. In Proceedings of the 2021 28th IEEE International Conference on Electronics, Circuits, and Systems (ICECS), Dubai, United Arab Emirates, 28 November–1 December 2021; pp. 1–5.
32. Moiselto, E.; Bonizzoni, E.; Malcovati, P. A 0.756-ppm/°C Time-Domain-Based Curvature-Compensated Bandgap Reference. In Proceedings of the 2023 IEEE International Symposium on Circuits and Systems (ISCAS), Monterey, CA, USA, 21–25 May 2023; pp. 1–5.

33. Pereira, M.S.; Costa, J.E.N.; Santos, M.; Vaz, J.C. A 1.1  $\mu$ A voltage reference circuit with high PSRR and temperature compensation. In Proceedings of the 2015 Conference on Design of Circuits and Integrated Systems (DCIS), Estoril, Portugal, 25–27 November 2015; pp. 1–4.
34. Qu, J.; Wu, C. A low temperature coefficient wide temperature range bandgap reference with high power supply rejection. *IEICE Electron. Express* **2023**, *20*, 20230104. [[CrossRef](#)]

**Disclaimer/Publisher’s Note:** The statements, opinions and data contained in all publications are solely those of the individual author(s) and contributor(s) and not of MDPI and/or the editor(s). MDPI and/or the editor(s) disclaim responsibility for any injury to people or property resulting from any ideas, methods, instructions or products referred to in the content.